Highly Porous TiO_2 Anatase Optical Thin Films with Cubic Mesostructure Stabilized at 700 °C

David Grosso,[†] Galo J. de A. A. Soler-Illia,[†] Eduardo. L. Crepaldi,[†] Florence Cagnol,[†] Christophe Sinturel,[‡] Alexis Bourgeois,[§] Aline Brunet-Bruneau,[§] Heinz Amenitsch,[||] Pierre A. Albouy,[⊥] and Clément Sanchez*,[†]

Laboratoire de Chimie de la Matière Condensée, Université Pierre et Marie Curie, CNRS UMR 7574, 4 place Jussieu, 75 252 Paris Cedex 05, France, Centre de Recherche sur la Matière Divisée, 1b rue de la Ferollerie, 45 071 Orléans Cedex 02, France, Laboratoire d'Optique des Solides, Université Pierre et Marie Curie, 4 place Jussieu, 75 252 Paris, France, Institute of Biophysics and X-ray Structure Research, Austrian Academy of Sciences, Steyrergasse 17/VI, 8010 Graz, Austria, and Laboratoire de Physique des Solides, Université Paris-Sud, 91405 Orsay, France

Received March 26, 2003. Revised Manuscript Received September 9, 2003

TiO_2 optical thin films stable to 700 °C, exhibiting 35% volume porosity, more than 100 $m^2 \cdot g^{-1}$ in surface area, fully nanocrystalline anatase framework, and organized mesostructure (cubic *Im*3*m* derived), have been stabilized by careful delayed rapid crystallization (DRC) thermal treatments. In-situ time-resolved SAXS and WAXS investigations were simultaneously performed during such treatments. They revealed that a slow and progressive heating to a temperature just below that of the formation of anatase ($T_c \approx 400$ °C), followed by a long pretreatment at this temperature, stabilizes the amorphous network. A following rapid increase of temperature up to temperatures as high as typically 700 °C, followed by a short residence time at this high temperature, provokes the homogeneous formation of crystalline small nanoparticles and the total elimination of organic residues. The crystallization is accompanied by matter migration through diffusing sintering and pore merging along the [111] directions of the cubic structure, leading to a novel grid-like mesostructure with open porosity. This DRC treatment allows the preparation of highly porous and crystalline anatase films, with thermal stability 200 °C higher than previously reported, that are ideal for energy transfer applications. This emphasizes the role of the treatment method to stabilize transition metal oxide mesoporous materials over extended crystallization at high temperatures. These films exhibit excellent long time stability below 500 °C.

Introduction

Because of its physicochemical properties that combine hardness, chemical inertia, and optical and electronic activities, crystalline titania is an extremely attractive material for a great variety of applications which mainly concerns pigments, photo catalysis, and energy conversion.[1] Such latter applications require thin films processing (e.g., solar cells, sensors, etc.), and high surface area, high porosity, and high purity to optimize the device efficiency. Previous investigations focused on the classical deposition and sintering of small titanium oxide based intermediates (i.e., nanoparticles, clusters, or oligomers).[2] An alternative synthesis strategy, leading to a continuous TiO_2 organized network of controlled porosity is now available. It involves the template approach that was first introduced by the researchers of Mobil Co.[3] on silica, adapted to copolymer blocks[4] and to transition metal oxides,[5,6] and finely processed in thin films,[7,8,9] following the evaporation-induced self-as-

* To whom correspondence should be addressed. E-mail: clems@ccr.jussieu.fr.

[†] Laboratoire de Chimie de la Matière Condensée, Université Pierre et Marie Curie, CNRS UMR 7574.

[‡] Centre de Recherche sur la Matière Divisée.

[§] Laboratoire d'Optique des Solides, Université Pierre et Marie Curie.

[||] Austrian Academy of Sciences.

[⊥] Université Paris-Sud.

(1) Hagfeldt, A.; Grätzel, M. *Chem. Rev.* **1995**, *95*, 45.

(2) Gerfin, T.; Grätzel, M.; Walder, L. *Prog. Inorg. Chem.* **1997**, *44*, 345.

(3) (a) Kresge, C. T.; Leonowicz, M. E.; Roth, W. J.; Vartuli, J. C.; Beck J. S. *Nature* **1992**, *359*, 710. (b) Beck, J. S.; Vartuli, J. C.; Roth, W. J.; Leonowicz, M. E.; Kresge, C. T.; Schmitt, K. D.; Chu, C. T.-W.; Olson, D. H.; Sheppard, E. W.; McCullen, S. B.; Higgins, J. B.; Schlenker, J. L. *J. Am. Chem. Soc.* **1992**, *114*, 10834.

(4) (a) Huo, Q.; Margolese, D. I.; Ciesla, U.; Demuth, D. G.; Feng, P.; Gier, T. E.; Sieger, P.; Firouzi, A.; Chmelka, B. F.; Schüth, F.; Stucky, G. D. *Chem. Mater.* **1994**, *6*, 1176. (b) Zhao, D.; Feng, J.; Huo, Q.; Melosh, N.; Fredrickson, G. H.; Chmelka, B. F.; Stucky, G. D. *Science* **1998**, *279*, 548. (c) Zhao, D.; Huo, Q.; Feng, J.; Chmelka B. F.; Stucky G. D. *J. Am. Chem. Soc.* **1998**, *120*, 6024.

(5) (a) Yang, P.; Zhao, D.; Margolese, D. I.; Chmelka, B. F.; Stucky, G. D. *Nature* **1998**, *395*, 583. (b) Yang, P.; Zhao, D.; Margolese, D. I.; Chmelka, B. F.; Stucky, G. D. *Chem. Mater.* **1999**, *11*, 2813.

(6) Soler-Illia, G. J. de A. A.; Sanchez, C. *New J. Chem.* **2000**, 493.

(7) (a) Grosso, D.; Balkenende, A. R.; Albouy, P. A.; Ayral, A.; Amenitsch, H.; Babonneau, F. *Chem. Mater.* **2001**, *13*, 1848. (b) Soler-Illia, G. J. de A. A.; Crepaldi, E. L.; Grosso, D.; Durand, D.; Sanchez, C. *Chem. Commun.* **2002**, 2298.

(8) Grosso, D.; Soler-Illia, G. J. de A. A.; Babonneau, F.; Sanchez, C.; Albouy, P. A.; Brunet-Bruneau, A.; Balkenende, A. R. *Adv. Mater.* **2001**, *13*, 1085.

10.1021/cm031060h CCC: $25.00
Published on Web 10/24/2003

sembly (EISA) method.[10] Since then, great efforts have been dedicated to understanding the self-assembly and condensation mechanisms associated with the chemical and processing conditions applied during the preparation of such films.[11] High-quality mesoporous TiO_2 anatase thin optical films can now be easily and reproducibly prepared by this method. This approach was well-developed in previous papers,[6,8,12] and involves the liquid deposition of a solution containing the TiO_2 precursors, and surfactant molecule templates. After solvent evaporation, the surfactant micelles are trapped within the inorganic network. The porous material is obtained after condensation of TiO_2 and decomposition of the organic surfactant achieved by thermal treatment. For transition metal oxide materials, this latter thermal treatment step is critical because it induces the crystallization of the network. Indeed, the crystallization of TiO_2 into anatase is known to be initiated around 400 °C and is often accompanied by the porosity collapsing and the formation of a dense film.[13] However, such a dramatic finality can be eluded if a careful treatment is applied. The present article is dedicated to the role of the thermal treatment conditions on the morphological change induced on a body centered cubic porous structure of TiO_2 films during crystallization. This study is based on in-situ, time-resolved small- and wide-angle X-ray scattering (SAXS and WAXS) investigations, simultaneously performed during thermal treatment of the latter films in various conditions. This study shows that the temperature program applied during treatment is critical because it affects the whole film morphology at the meso- and micro-scales through the network shrinkage and crystallization, respectively. It also confirms that the mesoporous structure is greatly affected by the crystallization of the TiO_2 network. Indeed, previous works reported thermal stabilities up to 400 °C, which is very close to T_c.[8,13,14] We show here that the network meso-organized periodicity, fully composed of anatase nanocrystals, can be retained with 35% volume of porosity above 650 °C when applying a specific careful treatment addressed as the delayed rapid crystallization(DRC) treatment. The microstructure was confirmed by high-resolution transition electronic microscopy (HRTEM). The porosity and the film atomic composition were estimated from combined Rutherford Back Scattering (RBS) analysis and optical properties measured by Variable Angle Spectroscopic Ellipsometry (VASE).

Table 1. Maximal Unidirectional Contraction (C_{max}), Temperature of Anatase Formation (T_c), and Temperature of Mesostructural Stability (3-Dimensional Cohesion) (T_s), Deduced from WAXS and SAXS Data during Heating in Various Conditions Given as the Pretreatment (PT) Conditions and the Following Heating Rate (X)

samples	PT conditions	X (°C/min)	C_{max} (%)	T_c (°C)	T_s (°C)
F10	aged 5 h at 25 °C	10	68	460	570
F20		20	66	420	520
PT10	4 d at 60 °C + 12 h at 100 °C + 12 h at 300 °C + 30 d at 25 °C	10	64	500	680
PT20 (DRC[a])		20	62	560	710

[a] DRC stands for the optimized conditions of delayed rapid crystallization treatment applied to the PT20 samples.

Experimental Section

Thin hybrid meso-organized TiO_2 films were prepared as previously reported:[8] ultrathin (10−20 μm) silicon wafer substrates were withdrawn from a solution containing $TiCl_4$/H_2O/EtOH/$HO(CH_2CH_2O)_{106}(CH_2CH(CH_3)O)_{70}(CH_2CH_2O)_{106}H$ (Pluronic F127) (1:10:40:0.005 molar ratio) after homogenization. If deposited with the proper humidity sequence of 40% during evaporation and 60% during the following hours, the film exhibits an excellent optical transparency and a body centered cubic mesostructure ($Im3m$)[15] with an initial lattice parameter a of 18 nm deduced from the SAXS patterns. Films were then simultaneously analyzed by SAXS and WAXS when heat treated from 25 to 750 °C following four different protocols listed in Table 1. Some films were pretreated (Samples PTX) while some were directly brought to the maximal temperature of 750 °C (Samples FX), where X stands for the heating rates. PTX films underwent a pretreatment composed of successive journeys at increasing temperatures up to 300 °C. The in-situ SAXS−WAXS experiment schemed in Figure 1 was performed at the SAXS-beamline of the third generation synchrotron ELETTRA (Italy), delivering the high flux of 8 keV necessary for such an experiment. Fresh (FX) or pretreated (PTX) films were disposed in the center of a specially designed furnace capable of heating at the rates of $X = 10$ or 20 °C min^{-1}, and equipped with apertures designed to allow the incident, the diffused, and the diffracted radiations in and out of the heating device without hindrance. The incident angle was fixed at 5±1° with the film surface to eliminate the specular reflection and the Yoneda signal from the detectors.[11] The 2D-CCD camera was placed to collect the global SAXS patterns every 2 min (10 s acquisition), while the linear detector was located at the position of the anatase first and most intense (101) diffraction and collected one diagram every 2 min (120 s acquisition) during temperature raise. The meso- and microstructures were then deduced from 2D and 1D diffraction patterns, respectively. The same films were additionally characterized by high-resolution transition electronic microscopy (HRTEM) (JEOL 100 CX II) Rutherford back scattering (RBS) from which the number of atoms per film volume unit and film porosity can be assessed with 10% error. VAS-Ellipsometry (SOPRA) investigations provided the optical constants of films at various temperatures of treatment. Corresponding surfactant-free systems were analyzed to determine network wall refractive index.

Results and discussions

SAXS and WAXS Data Recorded on a Fresh Film Thermally Treated at 10 °C min^{-1}. A typical WAXS diagram evolution with temperature, obtained for the F10 sample (fresh without pretreatment at 10 °C min^{-1})

(9) Crepaldi, E. L.; Soler-Illia, G. J. de A. A.; Grosso, D.; Sanchez C. *New J. Chem*. **2003**, *27*, 9.
(10) Brinker, C. J.; Lu, Y.; Sellinger, A.; Fan, H. *Adv. Mater*. **1999**, *11*, 579.
(11) (a) Grosso, D.; Babonneau, F.; Albouy, P. A.; Amenitsch, H.; Balkenende, A. R.; Brunet-Bruneau, A.; Rivory, J. *Chem. Mater*. **2002**, *14*, 931. (b) Grosso, D.; Balkenende, A. R.; Albouy, P. A., Ayral, A.; Amenitsch, H.; Babonneau, F. *Chem. Mater*. **2001**, *13*, 1848. (d) Soler-Illia, G. J. de A. A.; Grosso, D.; Crepaldi, E. L.; Cagnol, F.; Sanchez, C. *Mater. Res. Soc. Symp. Proc. (Hybrid Inorganic−Organic Materials)* **2002**, *726*, 243. (c) Grosso, D.; Babonneau, F.; Sanchez, C.; Soler Illia, G. J. de A. A.; Crepaldi, E. L.; Albouy, P. A.; Amenitsch, H.; Balkenende, A. R.; Brunet-Bruneau, A. *J. Sol-Gel Sci. Technol*. **2003**, *26*, 561.
(12) Soler-Illia, G. J. de A. A.; Scolan, E.; Louis, A.; Albouy, P. A.; Sanchez, C. *New J. Chem*. **2001**, *25*, 156.
(13) Schüth, F. *Chem. Mater*. **2001**, *13*, 3184.
(14) Alberius, P. C. A.; Frindell, K. L.; Hayward, R. C.; Kramer, E. J.; Stucky, G. D.; Chmelka, B. F. *Chem. Mater*. **2002**, *14*, 3284.
(15) Soler-Illia, G. J. de A. A.; Crepaldi, E. L.; Grosso, D.; Durand, D.; Sanchez, C. *Chem. Commun*. **2002**, 2298.

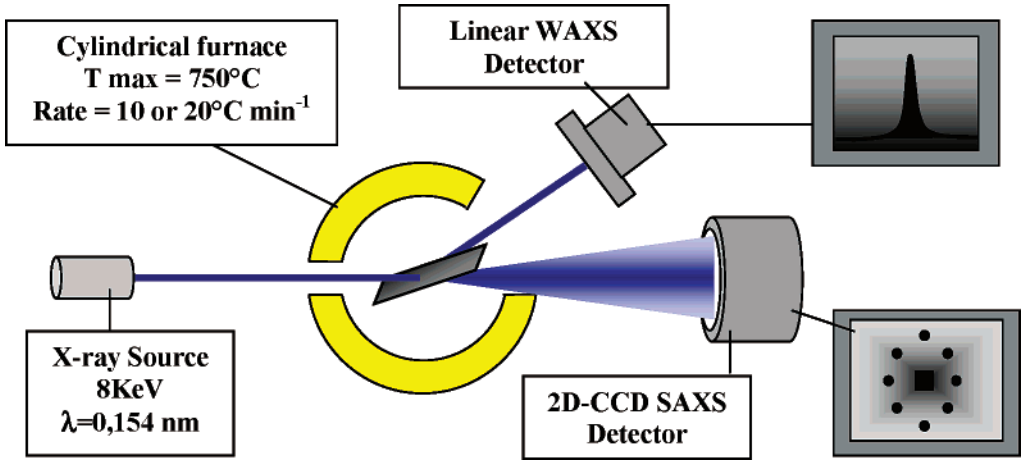

Figure 1. Scheme of the in-situ time-resolved simultaneous SAXS and WAXS investigations performed on TiO_2 films in various thermal treatment conditions.

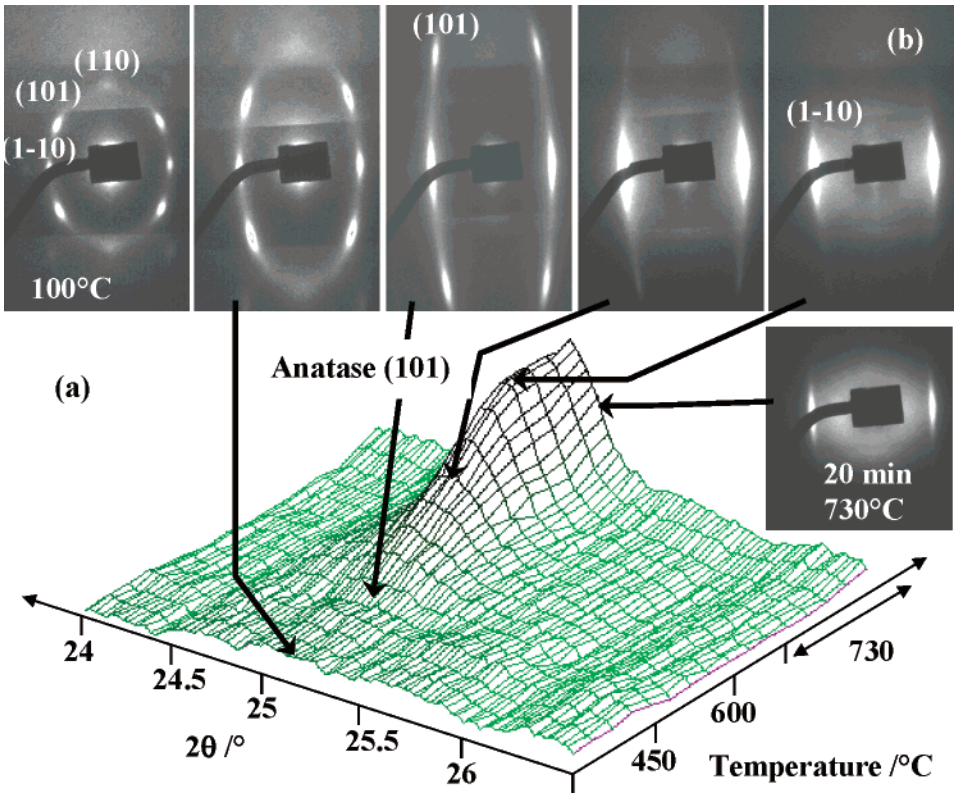

Figure 2. WAXS (a) and SAXS (b) raw data obtained during thermal treatment of a F10 sample (fresh film heated at 10 °C min^{-1}).

is shown in Figure 2(a), together with the corresponding 2D-SAXS patterns in Figure 2(b). The WAXS diagram evolution shows that no diffraction related to the presence of anatase particles is recorded below the critical temperature of crystallization, $T_c = 460$ °C, in the F10 conditions. From T_c, the (101) anatase peak starts to appear and increases in intensity. The maximal temperature permitted by the oven (i.e., 730 °C) was then maintained for 20 min before ending the experiment. This suggests that in such conditions, nanoparticles start to form above 450 °C and grow progressively in size by sintering with increasing temperatures. Above 700 °C, one expects the network to be fully composed of these crystalline entities as no more evolution is recorded. The final crystalline particle average dimension was estimated from the full width at half maximum (fwhm = $\Delta 2\theta$) of the (101) anatase peak to be around 30 nm (the anatase (101) peak did not significantly narrow at high temperatures and $\Delta 2\theta$ value evolved around 0.25°). However, this value must be handled with care because the peak shape is directly related to the size of the incident beam, to the angle of incidence, and to the sample dimension in the present experimental geometry. Therefore, one cannot precisely follow the nanoparticle size evolution with temperature, and the 30-nm value is likely to be overestimated at lower temperatures and underestimated at higher temperatures. We will see later by HRTEM investigations that particles are effectively smaller at 500 °C than at 730 °C. No diffraction peaks corresponding to the brookite or rutile structures of TiO_2 were recorded in these conditions.

Regarding the SAXS data, the initial pattern is composed of mainly three peaks that correspond to the (110), (101), and (1$\bar{1}$0) miller indices of planes of a body centered cubic (*Im*3*m*) structure with domains preferentially oriented with the [110] direction normal to the surface, and allowed by the circular permutation. The corresponding initial lattice parameter (*a*) was deduced to be 18 ± 1 nm. The lower intensity of the (110) peak is due to the incident angle of 5° that reduces the quantity of domains having their in-plane diffraction in the Bragg conditions. This structure has been well detailed in previous works.[15] The contraction of the domains can be calculated from the position of the (101) peak because this latter has an in-plane and an off-plane component. The typical unidirectional mesostructure shrinkage in the (110) direction (in-plane), commonly observed during drying/calcinations of thin films, is well characterized by the vertical extension of the pattern.[16] In the conditions of F10, the maximal in-plane contraction measured before disappearance of the (101) diffraction was 68% at T_s = 570 °C. T_s is associated to the disappearance of the (101) peak, and will then assess the limit of the three-dimensional cohesion. In other words, it is the temperature at which the structure loses its integrity. On the other hand, no contraction is observed in the directions of the film surface plane (off-plane), suggesting that the periodicity is entirely retained in the (1$\bar{1}$0) directions up to the maximal available temperature of 730 °C. Extending the residence time at this temperature (typically more than 1 h) results in the progressive but slow loss of the (1$\bar{1}$0) peak without contraction. An additional observation concerns the peak intensity evolution. Indeed, when the temperature reaches the value of T_c, which was experimentally determined at 460 °C for the F10 sample, the (10$\bar{1}$) peak intensity dramatically increases while the (1$\bar{1}$0) peak intensity inversely decreases. During crystallization, the electronic density of the titania framework slightly increases, but this cannot be the main reason for the sudden peak intensity variations because it would have generated a general increasing of the spot intensity and not the observed relative opposite variation. This phenomenon can thus only be related to a morphological change at the mesoscopic level that took place just after crystallization of the network. In addition, the loss of the mesostructure 3D cohesion, corresponding to T_s = 570 °C here, is accompanied by the sudden and fast decreasing of the (1$\bar{1}$0) off-plane peak intensity.

Interestingly, the global behavior of films (all four samples) was deduced from the related SAXS and WAXS data to be similar toward each of the four different applied thermal treatments (see Table 1). Only critical T_c and T_s values differed. Concerning the lattice contraction, the in-plane and off-plane evolutions with temperature reported in Figure 3 show that the same unidirectional contraction applied for both heating rates. Although the off-plane periodicities are not influence by the temperature, the in-plane ones undergo a constant shrinkage up to 260 °C, which is followed by a faster shrinkage between 260 and 320 °C that is related to the thermal decomposition of the Pluronic F127. The contraction is then relatively stabilized up to the temperature of peak disappearance (T_s). Films that were pretreated at 300 °C (PT) have a greater stability as illustrated by lower in-plane contraction and higher T_s. Indeed, in-plane (101) peaks are still observable above 700 °C for PT films but never survive at 600 °C when not pretreated at 300 °C. This better stability is also demonstrated in Table 1 and in Figure 4, where the variations of peak intensity are given for each treatment condition. It is clear that T_c and T_s values are greater for pretreated films than for fresh films. This suggests once more that the treatment conditions do influence the evolution of the micro- and mesostructures. As already mentioned for F10, the splitting point of in-plane and off-plane intensity similarly corresponds to the observed temperature of anatase formation (T_c) for any conditions (i.e., F10, F20, PT20, and PT10). The zone delimited by T_c and T_s represents the temperature range within which the network crystallizes in anatase nanoparticles but within which the mesoporosity does not collapse and remains entirely 3D-meso-organized. This zone is wider and located at higher temperatures for pretreated films, once more emphasising the higher thermal stability brought by the pretreatment at 300 °C. Another interesting observation is made by comparing the T_c and T_s values in Table 1. Without pretreatment, higher stability (higher T_c and T_s) is favored by lower rate of heating. On the other hand, higher stability is inversely favored by higher rate of heating if the pretreatment is applied. To summarize, the longer the system undergoes the 300 °C pretreatment, the greater the energy is needed to crystallize the network and to make it collapse in a second step. Therefore, the best thermal stability, observed with PT20, is attributed to the long pretreated systems to which the energy of crystallization is rapidly brought in a second step by a fast heating rate.

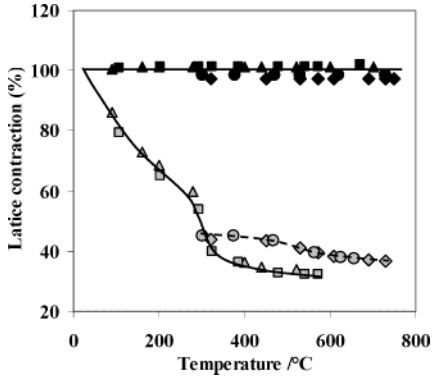

Figure 3. In-plane (grey) and off-plane (black) contraction recorded by SAXS with temperatures: square (■), F10; triangle (▲), F20; circle (●), PT 10; and lozenge (♦), PT20.

For such systems, it is known that the rigidification of the initial amorphous inorganic network is related to the condensation reactions between Ti−oxo generated intermediate species. Indeed, the greater the number of Ti−O−Ti oxo bonds is, the greater is the stiffness of the amorphous materials. The transformation into anatase requires enough energy to rearrange these entities into quadratic lattice of octahedral unities linked throughout their edges (O-μ3 only). If the initial amorphous material is already well stabilized by a high

(16) (a) Grosso, D.; Balkenende, A. R.; Albouy, P. A.; Lavergne, M.; Mazzerolles, L.; Babonneau, F. *J. Mater. Chem.* **2000**, *10*, 2085. (b) Kundu, D.; Zhou, H. S.; Honma, I. *J. Mater. Sci. Lett.* **1998**, *17*, 2089.

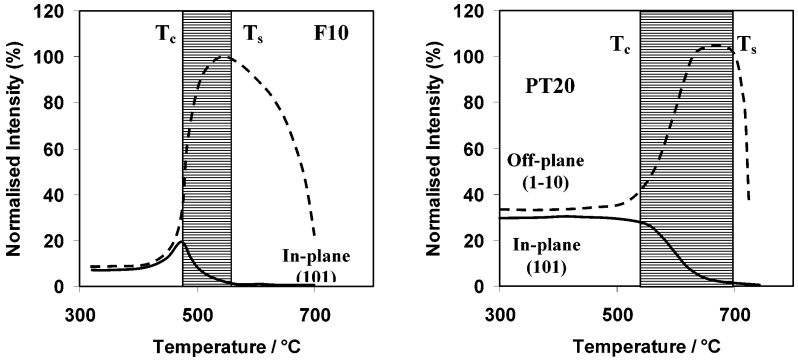

Figure 4. Off-plane and in-plane diffraction peak intensity versus temperature for the F10 and PT20 samples.

degree of cross linking induced by a long period of time at temperatures just below the temperature of anatase crystallization ($T_{anatase} \approx 400$ °C), more quantity of energy is require for the crystallization. This quantity of energy can be brought to the system in two ways: (i) a long period of time at temperatures just above $T_{anatase}$ (represented by the PT10 conditions) which is accompanied by lower mesostructure stability ($T_s = 680$ °C) or (ii) a shorter period of time at temperature far above $T_{anatase}$ (represented by the PT20 conditions) and accompanied by greater mesostructure stability ($T_s = 710$ °C). The better mesostructure stability, observed with the more rapid thermal treatment that followed a long pretreatment at 300 °C (PT20), is attributed to the energy over-saturation phenomenon that favors fast formation of small anatase particles. This fast treatment, addressed as the delayed rapid crystallization (DRC) treatment, induces a rapid and homogeneous braking of the amorphous cohesion and allows a fast reorganization of atoms into small nuclei, and then into nanoparticles of crystals that cannot distort the mesostructure too much by their restricted size. Also such DRC treatment sequence promotes particle monodispersion in size. Periods of thermal crystallization that are too long result in the dramatic sintering of these particles into large ones responsible for the mesostructure collapsing.

Film Structures as Revealed by HRTEM. Figure 5 displays the electronic microscopy images of TiO_2 based films treated at 100 °C for 12 h ((a) [100] zone axis, and (b) [111] zone axis), treated up to 500 °C (T_c) for 6 h following the PT10 conditions ((c) and (d) [110] zone axis, and (e) [1$\bar{1}$0] zone axis), and treated at 730 °C for 20 min following the PT20 conditions ((f) and (g)). For all samples, images are representative of the whole film structure confirming that layers are homogeneously structured. Pore distances measured on these are in agreement with the corresponding SAXS *d* spacing, with the precision allowed by the focusing the cutting and tilting angles associated with TEM (estimated at ± 15%). The most interesting remark concerns the mesostructure transformation that occurs between 100 and 500 °C. Indeed, at 100 °C the material contains only discrete well-separated spherical pores, whereas at 500 °C it is composed of gridlike (e) and layerlike (c) features, as if pores have merged in preferential directions. This transformation is characterized by the SAXS pattern evolution after T_c, where the in-plane (10$\bar{1}$) peak decreases in intensity while the off-plane (1$\bar{1}$0) one increases in intensity. The second interesting observation concerns the crystallinity of the structure as

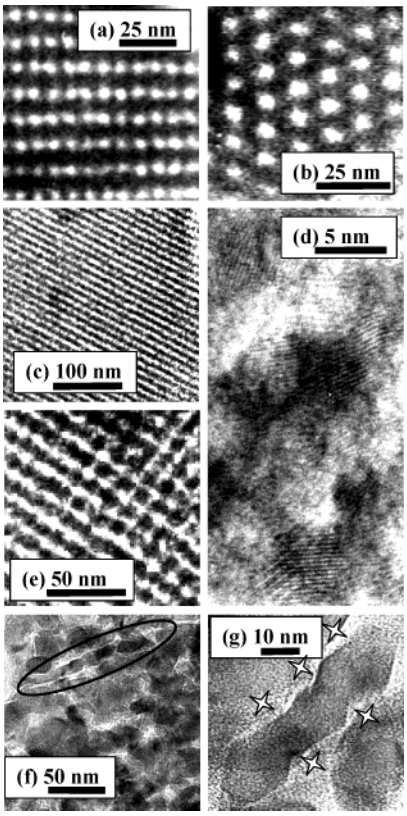

Figure 5. HRTEM images of TiO_2-based films treated at 100 °C for 12 h ((a) [100] zone axis, and (b) [111] zone axis); treated up to 500 °C (T_c) for 6 h following the PT10 conditions ((c) and (d) [110] zone axis, and (e) [110] zone axis); and treated at 730 °C for 20 min following the PT20 conditions ((f), and (g) enlargement of (f)). The white stars indicate the pore positions in the initial structure.

evidenced in image (d) where less than 10 nm in side anatase particles with their reticular plans are clearly visible all over the sample. Because samples are mechanically prepared (physically ground and microtomed) crystalline particles are dispatched, but still one can make out pore areas (white regions). It is clear that after 6 h at 500 °C (DRC method) the film is totally composed of highly crystalline anatase nanoparticles, elemental bricks of the still well-organized mesoporous network. More interestingly, no mesostructure change occurred during the 500 °C 6 h treatment. After 20 min at 730 °C, the latter clear meso-organizations are no longer visible. Instead, more than 20-nm size anatase aggregated particles are observed, suggesting that the meso-organization is being progressively dismantled by further sintering of small particles into larger ones.

Table 2. RBS and VASE Results Corresponding to a PT20 Sample at Various Temperatures along the Treatment Process

sample DRC		Ti[a]	O/Ti[a]	C/Ti[a]	P_{RBS}[b] (%)	n_{VASE} F[c]	n_{VASE} W[c]	P_{VASE}[b] (%)
300 °C	amor.	1.73×10^{22}	2	0.7	40	1.75	2.18	45
500 °C[d]	cryst.					1.85	2.27	35
730 °C	cryst.	2.10×10^{22}	1.8	0.1	28	1.89	2.32	35

[a] RBS atoms contained are given in number of atoms per cm^{-3} for Ti, and in molar ratio for C and O with 10% error. [b] P_{RBS} and P_{VASE} are porous volumes deduced from both RBS and VASE techniques with 10% error (RBS error) and 5% error (Bruggeman effective medium approximation model), respectively. [c] Optical constants n_{VASE} F (for film samples) and n_{VASE} W (for network walls) obtained by VASE are given for $\lambda = 600$ nm. [d] The 500 °C sample stood 12 h at this temperature.

However, a careful look at these particles reveals that their shape (Figure 5(g)) and their arrangement (Figure 5(f) elliptical zone) have kept the "memory" of the initial and intermediate structures (also verified by the presence of the off-plane diffraction at high temperatures in Figure 2(b)). Indeed, Figure 5(f) shows an elongated string of particles recalling the same array and dimension as that shown in image (c). The best example stands in image (g) and shows a 10-nm wide and 50-nm long anatase single particle whose shape and dimension perfectly fit the initial and intermediate structures virtually represented here by the locations of the initial spherical pores as white stars. This insinuates that the morphological change associated with the epithaxial nucleation/association of small particles into larger ones is influenced by the porous organization. Two delicate questions have to be answered at this point. What is the limit of crystallization degree after which the mesostructure is no longer stable?; and what are the characteristics of this limit?

RBS and VASE Investigation. From what is reported above, the conditions of thermal treatment applied to such mesostructured titania-based films determine the mesostrcuture and microstructure of the film. It is now possible to prepare crystalline TiO_2 films stable to 700 °C. For interesting applications, these have to exhibit a high porosity that, when combined with the present mesostructure, is associated with a high surface area and thus a great surface of exchange. The characterization of thin film porosity has always been a challenge as it involves a very low quantity of matter. The best method combines the RBS data on the quantity of atom per surface of film and the optical properties deduced from ellipsometry investigations.[7]

RBS and VASE final treated results are given in Table 2. The variation of the quantity of titanium per volume between 300 and 730 °C is related to the contraction of the structure as also observed by SAXS. Taking into account the error, the variation of oxygen atom per Ti is coherent, confirming that the TiO_2 stoichiometry is close at low temperatures and is reached during crystallization, as expected. The high quantity of C at low temperature results from the thermal degradation of the copolymer block and is likely to be combined with O into carbonate species. These are eliminated at high temperatures as the C/Ti = 0.1 is within the error range and may also be related to pollutant adsorption within the network. Thus, a DRC treatment brought to 700 °C allows for the formation of pure anatase networks. Related calculation of the porosity P_{RBS} shows that the porous volume is only slightly reduced from 40 to 28% between 300 and 730 °C. The band gap (BG) measured by ellipsometry on films that were DRC treated between 500 and 700 °C was 3.4 eV (± 0.1depending on the fitting) and is in accordance with anatase particles of less than 10-nm size.[17] The refractive indices were measured for corresponding networks with and without surfactant to assess the porosity related to the template, through the Bruggeman effective medium approximation. Refractive indices have globally lower values than that of pure anatase materials as a result of the presence of C and potential microporosity. The mesoporosity values were slightly higher than that deduced from RBS but remained within the error range. A theoretical calculation of the specific surface area (SA), taking an average porosity of 40 vol %, the density $\rho = 3.89$ of the crystalline TiO_2, and an average pore diameter of 7 nm, gives SA = 100 $m^2 \cdot g^{-1}$. Of course, this value is underestimated because it does not take into account the potential microporosity and the roughness of the pore walls. In summary, DRC treatments above the temperature of crystallization and up to 700 °C lead to films exhibiting the interesting charge-transfer properties together with high purity, high optical quality, high meso-organization, high porosity, and high surface of exchange.

From the Amorphous Cubic Mesostructure to the Nanocrystalline Meso-Organized Porosity. The historical of mesostructuration evolution with temperature is deduced from the in-situ SAXS and WAXS data and is illustrated in Figure 6. Part (a) summarizes how the initial *Im*3*m* (bcc) cubic structure transforms first into the P1 (bc) triclinic structure upon unidirectional contraction, and in a second step into the two-dimensional grid-like structure upon pore merging as observed in TEM of Figure 5(e). In these representations, the substrate is normal to the Figure plane. Along the structural transformation process, (abc) axes remain the same and are submitted to the same unidirectional contraction than the lattice for clarity. Part (b) represents two typical different views of the structure before (DRC) treatment. The [110] view shows the top surface of the film (the substrate lays below in the image plane). The [111] view shows the contracted structure in the direction of the c_6 axis of the formal body centered cubic structure. Distances between the pores are defined by the lattice parameter a, but vary depending on the degree of unidirectional contraction (C_{max}). Characteristic distances between four characteristic pores labeled W, X, Y, and Z are given versus C_{max} in Figure 6(c), where $YZ = a((\sqrt{3})/2)$; $XW = a(\sqrt{2})((100 - C_{max})/100)$; $XZ = (a/\sqrt{2}) \times \sqrt{(1 + ((100 - C_{max})/100)^2)}$; and $XY = (a/2) \times \sqrt{(1 + 2((100 - C_{max})/100)^2)}$. In relation to this diagram, XY is the smallest distance between two pores in the lattice from 0% up to 60% contraction, signifying that thinner walls (less matter) sit between these two

(17) Koelsch, M.; Cassaignon, S.; Guillemoles, J. F.; Jolivet, J. P. *Thin Solid Films* **2002**, *403*, 312.

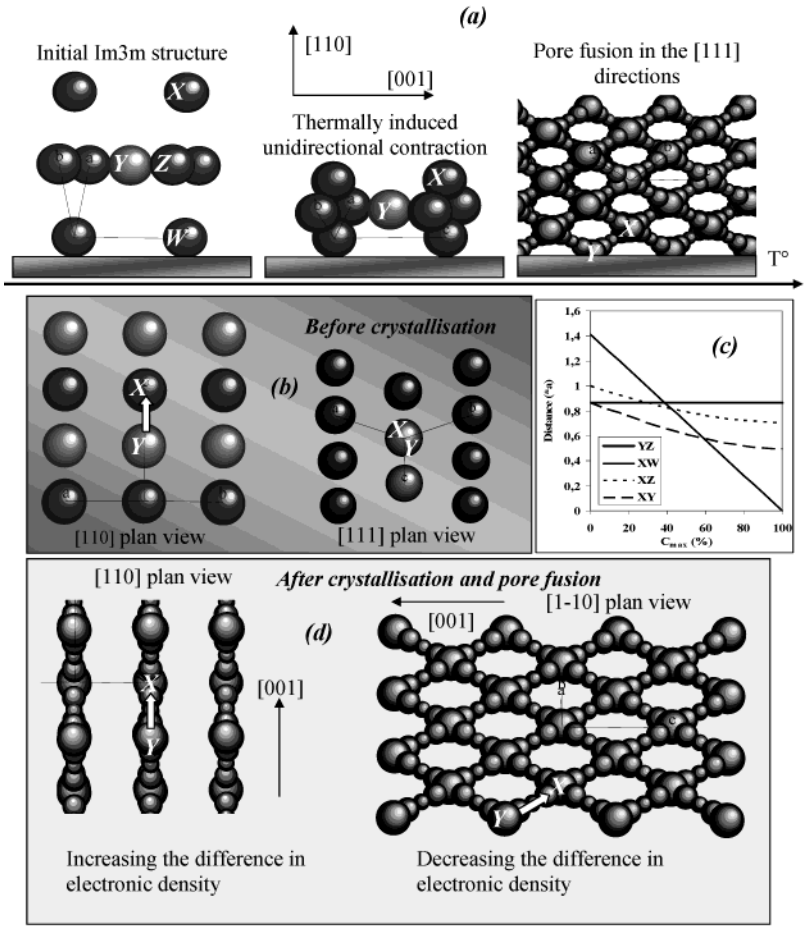

Figure 6. Scheme representing the structural variation during the various steps of heat treatment.

pores. This "pore richest" *XY* direction is an important one because it corresponds to the [111] direction of the cubic or triclinic structures also represented by the white arrows in Figure 6(b) and (d). This direction is also that of the epithaxial relation, existing between the *Im*3*m* cubic structure and the *p*6*m* 2D-hexagonal structure.[18] This latter transition occurs through the merging of the micelles in the liquid crystalline state. Figure 6(d) shows the possible structure of the film after the DRC treatment, where pores have similarly merged within the *XY* "pore richest" directions. These are the [111] and [11$\bar{1}$] directions contained in the (1$\bar{1}$0) planes (see [1$\bar{1}$0] view plane) and are also those of the epitaxial relation detailed above. In Figure 6(d), the smaller spheres are illustrating the merging and their directions. What strongly suggests that pores merge during the DRC treatment are the TEM images in Figure 5(c) and (e), and the systematic inverted variations of the in-plane and off-plane peak intensity of Figure 4. Because this phenomenon cannot be related to the variation of the titania electronic density and to the form factor of the domains (i.e., the system remains a supported film), it can only be related to a variation of the structural factors of both in-plane and off-plane directions of diffraction. As a result, it can only be explained by a migration of the matter through diffusive sintering that simultaneously generates an increasing of amplitude in the electronic density profile of the (1$\bar{1}$0) diffraction and a corresponding extinction of the (110) and the (101) diffractions by progressive attenuation of the corresponding density profile amplitude. This mesostructure transformation can be chronologically explained as followed: from previous data the initial pore diameter can roughly be estimated at 7 nm, suggesting that when the lattice undergoes a contraction of more than 50%, some pores walls have considerably thinned. This is especially true between pores *XY* where less matter are present according to Figure 6(c). When T_c is reached, the physical cohesion of the amorphous framework is broken through the formation of nanoparticles of anatase. Their growth and nucleation is limited by the diffusion of matter and therefore is quenched at the porosity interface in a first step. These limited-in-size nanoparticles are denser than the amorphous initial network which implies the creation of gaps and results in an enhanced degree of mobility. In a second step, sintering carries on causing the matter to move from positive curvatures to negative curvatures as to minimize the surface-to-volume ratio. In other words, smaller particles migrate toward larger ones in order to fill the gaps. This phenomenon is called diffusive sintering and is driven by the minimization of the material surface energy.[19] Because small particles are preferentially formed within thinner walls (between the *X* and *Y* pores), the diffusion of matter takes place from between these *X* and *Y* pores toward surrounding denser regions.

(18) Sakya, P.; Seddom, J. M. M.; Templer, R. H.; Mirkin, R. J.; Tiddy, G. J. T. *Langmuir* **1997**, *13*, 3706.

(19) Brinker, C. J.; Sherer, G. W. *Sol−Gel Science*; Academic Press: London, 1990; p 724.

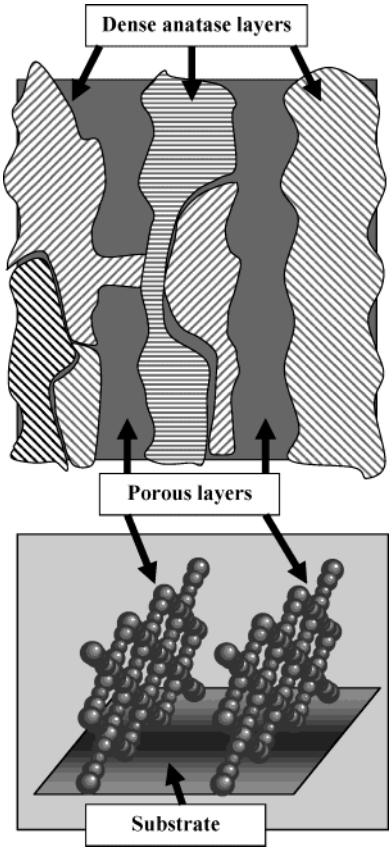

Figure 7. Scheme illustrating the final mesoporous crystalline structure.

The result is a merging of the pores in the [111] and [11$\bar{1}$] directions. The final structure would resemble the model of Figure 6(d). In such sintering-assisted rearrangement of matter, particles nucleate through formation of grain boundaries as is the case in Figure 5(f). But large single particles such as that of Figure 5(g) can be formed through epithaxial fusion/nucleation because no grain boundary is visible. This matter rearrangement is the only possible physical fact responsible for the disappearing of the in-plane diffraction and the simultaneous reinforcement of the off-plane one. The final structure can be illustrated as in Figure 7, where pore-rich grid-like layers intercalate, perpendicularly to the substrate surface, with dense layers of nanonatase aggregates. This is once more highlighted by the single anatase particle of Figure 5(g), which keeps under its morphology the memory of the initial structure, and which explains by itself that the direction of preferential nucleation originates from between *X* and *Y* pores. This structure can easily accommodate anatase nanoparticles with two dimensions, over three, greater than 10 nm. In addition, it has the advantage of exhibiting interconnected open porosity, directly linking both film interfaces, in contrary to the initial cubic structure and the classical *p*6*m* one. Extended periods of time at temperatures as high as 730 °C will obviously lead to the complete but progressive deterioration of the mesostructure by sintering. A careful DRC treatment performed as high as 700 °C will then stabilize the film for application below 600 °C as no mesostructural deterioration was observed below this upper limit temperature for PT10 and PT20 films.

Previous studies reported the formation of similar films with a slow and progressive treatment that involved a pre-consolidation between 60 and 130 °C, followed by the surfactant removal around 350 °C, followed by the crystallization below 500 °C. Collapsing of the structure was observed above 500 °C.[9] TiO_2 Brookite nanoparticles were found as intermediate species that are likely related to the different sequence of treatment applied in this latter step-by-step process (longer periods of residence at fractioned temperatures). The new concept described in the present study prevents the formation of intermediate Brookite and allows for a better limitation of the particle growth and thus a higher thermal stability (700 °C) compared to that of a step-by-step protocol (500 °C).

Conclusion

To summarize, the mechanisms involved during the thermal crystallization of mesoporous TiO_2 thin films have been understood through simultaneous SAXS and WAXS in-situ investigations. This globally shows that the growth of anatase particle can be controlled to prevent the mesostructure collapse. Indeed, a fast and short treatment at elevated temperature applied to the cubic initial mesostructure allows rapid growing of the Anatase particles up to the limit imposed by the mesostructure. Further annealing is then quenched by rapid temperature drop. The optimal thermal treatment conditions to obtain: (i) highly pure anatase nanoparticles (no rutile and organic residues); (ii) highly stable (short period at 700° C and extended period at 500 °C); (iii) highly porous (35 vol %); (iv) highly structured with narrow pore size distribution (7 nm); and (v) with an excellent optical quality and electron-transfer properties (BG = 3.4 eV), Anatase TiO_2 thin films are the following: a pretreatment composed of an as-long-as-possible period of time at a temperature just below crystallization (long stabilization plateau typically at 300 °C) must follow a slow and progressive raise to this latter temperature. It is then followed by a rapid increase of the temperature up to a temperature far above the crystallization one (typically 700 °C). A *short* period of time at this temperature is then required. The system will then present a very high thermal stability at temperatures below that of the rutile crystallization. In addition to its simplicity, this dynamic two-step delayed rapid crystallization treatment has the great advantage, over step-by-step treatment or direct calcinations, of allowing preparation of the material at a temperature as high as 700 °C, and to use them for applications at much more moderate temperatures such as below 500 °C for energy conversion (sensors, photocalysis, etc.). This method can be applied to many pure or mixed transition metal oxide mesoporous networks (e.g., films or powders such as Y or Ce modified ZrO_2,[20] TiO_2 spheres,[21] etc.) if the corresponding temperature of crystallization is known and if an amorphous mesostructured network can initially be formed.

(20) Crepaldi, E. L.; Soler-Illia, G. J. de A. A.; Bouchara, A.; Grosso, D.; Durand, D.; Sanchez, C. *Int. Angew. Chem.* **2002**, *3*, 347.
(21) Grosso, D.; Soler-Illia, G. J. de A. A.; Crepaldi, E. L.; Sanchez, C. *Adv. Func. Mater.* **2003**, *13*, 37.

Acknowledgment. The financial support from the European Community (funding ELETTRA synchrotron experiments) the French Ministry of Research, the CNRS, the CNPq (Brazil, grant 200636/00-0), and the Fundación Antorchas (Argentina) are greatly acknowledged. We thank Emma Grosso Camus for allowing access to modeling materials.

CM031060H